



FULL PAPER

Copper and nickel immobilized on cytosine@MCM-41: as highly efficient, reusable and organic–inorganic hybrid nanocatalysts for the homoselective synthesis of tetrazoles and pyranopyrazoles

Mohsen Nikoorazm | Bahman Tahmasbi | Shahab Gholami | Parisa Moradi

Department of Chemistry, Faculty of Science, Ilam University, Ilam, P.O. Box 69315516, Iran

Correspondence

M. Nikoorazm, Department of Chemistry, Ilam University, P.O. Box 69315516, Ilam, Iran.
Email: e_nikoorazm@yahoo.com

In this work, a green approach is reported for efficient synthesis of biologically active tetrazole and pyranopyrazole derivatives in the presence of Cu-Cytosine@MCM-41 and Ni-Cytosine@MCM-41 (copper (II) and nickel (II) catalyst on the modified MCM-41 using cytosine). The synthesis of tetrazoles and pyranopyrazoles in the presence of these catalysts was performed in green solvents such as water or poly (ethylene glycol) (PEG). All products were obtained in high TOF (turnover frequency) numbers in the presence of these catalysts, which indicate the high efficiency of these catalysts in the synthesis of tetrazole and pyranopyrazole derivatives. The prepared catalysts were characterized by various techniques such as BET, TGA, XRD, FT-IR, SEM, EDS, WDX, TEM, and AAS. Mesoporous structure of these catalysts was confirmed by nitrogen adsorption–desorption isotherms. These catalysts can be recovered and reused for several runs without significant change in their catalytic activity or metal capacity. The recovered catalysts have been characterized by XRD, SEM, EDS, WDX, FT-IR and AAS techniques, by which their heterogeneous nature has been confirmed.

KEYWORDS

copper (II), mesoporous MCM-41, nickel (II), pyranopyrazoles, tetrazoles

1 | INTRODUCTION

In recent years, there has been a rapid growth in the development of novel supported compounds such as supported catalysts, reagents, sensors and adsorbents.^[1–7] Therefore, nanoparticles have been widely used as solid supports for the immobilization of homogeneous catalysts.^[8–10] For example, silica materials,^[11] polymers,^[12] graphene oxide,^[13–16] carbon nanotubes,^[17] iron oxide,^[18] ionic liquids,^[19,20] boehmite nanoparticles,^[21,22] biochar,^[23] magnetic nanoparticles,^[24–26] etc. were employed as support for the stabilization of homogeneous catalysts. Among them, mesoporous silica materials, such as MCM-41, are inert in various chemical conditions as they have high stability in

aqueous solution, air atmosphere and high temperature. Large specific surface area (>1,000 m²/g) of MCM-41 including a lot of silanol groups leads to a simple modification of its surface which, in turn, would also lead to the high capacity of catalyst loading.^[27] High thermal stability of MCM-41 allows the application of MCM-41 in harsh condition of the organic reactions.^[28] Heterogeneity of MCM-41 allows the catalyst recycling supported on the surface of MCM-41. Moreover, the large specific pore volume of MCM-41 which is up to 1.3 ml/g allows supporting of huge organic ligands and metal complexes into its channels.^[29] Furthermore, MCM-41 is used in various fields such as catalysis, drug delivery systems,^[30] extraction,^[31] energy^[32] and adsorption.^[33] In this regard, we are reporting two

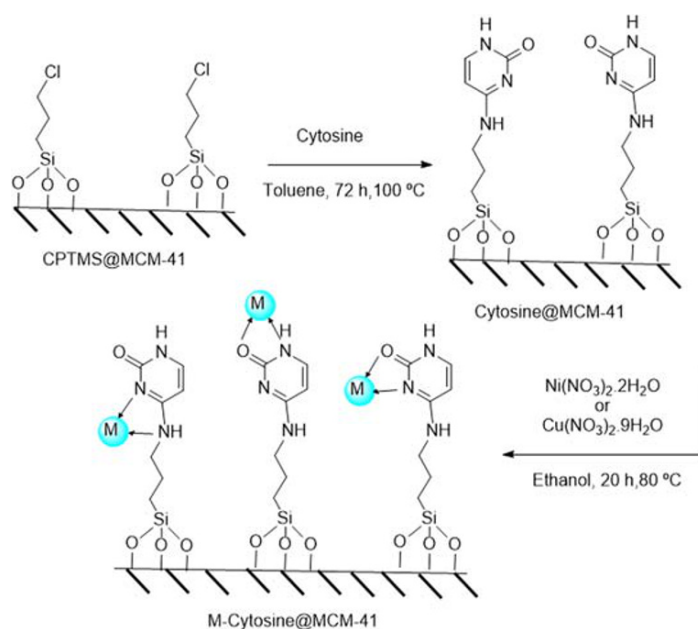
complexes of copper (II) and nickel (II) on MCM-41 as efficient and heterogeneous catalysts for the synthesis of tetrazole and pyranopyrazole derivatives.

Multicomponent Reactions (MCRs) are convergent reactions, in which more than two starting materials convert to the target product using a one-pot procedure without any separation of intermediates.^[34–40] The simplicity of procedure, high atom economy and time-saving are among the major advantages of MCRs.^[41–46] Therefore, MCRs have emerged as a powerful tool for the synthesis of biologically active and heterocyclic compounds from available starting materials without the need for purifying the intermediates.^[43,47–50] In this sense, pyranopyrazole derivatives can be synthesized from MCRs of aldehydes, malononitrile, hydrazine and ethyl acetoacetate. It is worth mentioning that Pyranopyrazoles are composed of pyrazoles and pyrans which are the very important classes of heterocyclic compounds. Pyranopyrazoles exhibit significant biological properties such as anticancer,^[51] antimicrobial,^[52] anti-inflammatory,^[53] molluscicidal activities,^[54,55] Chk1 kinase inhibitor,^[56] potential insecticidal,^[53] antiviral,^[54] vasodilator^[57] and analgesic.^[58] Likewise, tetrazole derivatives have been used in drugs i.e. used as analgesic, herbicidal, anti-HIV drug candidate, anti-proliferative, anti-inflammatory, antimicrobial, and anticancer agents.^[44,58–67] In this regard, TAK-456, olmesartan medoxomil, losartan and valsartan which are compounds possessing tetrazole ring have a biological activity such as antihypertensive family drugs.^[63,68] Therefore, we developed a simple catalytic procedure for the synthesis of pyranopyrazole and tetrazole derivatives.

2 | EXPERIMENTAL

2.1 | Materials and instruments

Chemicals and solvents as employed in this work were purchased from Aldrich, Fluka, or Merck companies and used without further purification. Thermogravimetric analyses (TGA) of the catalyst was recorded by a NETZSCH Simultaneous Thermal Analysis device under air atmosphere in the temperature range of 30–800 °C and at a heating rate of 10 °C min⁻¹. The morphology and size of the catalyst were obtained by TEM images using HRTEM-FEI TEC9G20 transmission electron microscope and SEM images using FESEM-TESCAN MIRA3 Scanning Electron Microscope. Moreover, this Scanning Electron Microscopes was employed for component elemental analysis (EDS and WDX) of nanoparticles. Besides, the exact content of copper and nickel in catalysts was measured by AAS technique using 400p-novAA instrument from Analytik Jena Company. Powder XRD patterns of the materials were performed with Cu K α radiation at 40 kV and 30 mA using a PW1730 instrument from Philips Company. Nitrogen adsorption isotherms were recorded by a standard gas manifold at 77 K to textural properties of the catalyst using a BELSORP MINI II device. In addition, the catalyst sample was degassed at 120 °C for 2 hr using a BEL PREP VAC II device before analysis. FT-IR spectra were recorded with KBr pellets using a VRTEX 70 model Bruker FT-IR spectrometer. NMR spectra of the products were recorded using Bruker DRX-400 spectrometer at 100–400 MHz. Melting points were measured with an Electrothermal 9,100 apparatus.



SCHEME 1 Preparation of Cu-Cytosine@MCM-41 and Ni-Cytosine@MCM-41

2.2 | Preparation of copper (II) or nickel (II) immobilized on mesoporous MCM-41 nanoreactor

Initially, the modified mesoporous MCM-41 nanoreactor by 3-chloropropyltrimoxysilane (CPTMS@MCM-41) was prepared based on a newly reported procedure.^[69] Subsequently, CPTMS@MCM-41 (1.0 g) was dispersed in toluene by sonication for 20 min and, then, 3 mmol (0.333 g) of cytosine was added to the reaction mixture. The obtained mixture was stirred for 72 hr at 100 °C. The solid product (cytosine@MCM-41) was isolated by simple filtration and washed with ethanol. In order to prepare Ni-Cytosine@MCM-41, 1.0 g of Cytosine@MCM-41 was dispersed in ethanol by sonication for 20 min and, then, mixed with 2 mmol (0.365 g) of Ni (NO₃)₂·6H₂O. Afterwards, the obtained mixture was stirred for 20 hr at 80 °C. This procedure is outlined in Scheme 1. Moreover, Cu-Cytosine@MCM-41 was prepared by stirring Cytosine@MCM-41 (1 g) and Cu (NO₃)₂·3H₂O (2 mmol, 0.483 g) in ethanol at 50 °C for 20 hr as outlined in Scheme 1.

2.3 | General procedure for the synthesis of 5-substituted 1H-tetrazoles

A mixture of NaN₃ (1.3 mmol, 0.845 g) and benzonitrile derivative (1 mmol) in the presence of Cu-Cytosine@MCM-41 (0.03 g, 3.1 mol%) or Ni-Cytosine@MCM-41 (0.03 g, 0.1 mol%) was stirred at 120 °C in poly ethylene glycol (PEG-400) as a solvent. After completion of the reaction [which was observed by thin-layer chromatography (TLC)], the catalyst was isolated by simple filtration then, the products were extracted by an aqueous solution of HCl (4 N) and ethyl acetate. The organic solvent was dried over

anhydrous sodium sulfate and, then, concentrated to give the crude solid product.

2.4 | General procedure for the synthesis of pyranopyrazoles compounds

A mixture of ethyl acetoacetate (1.0 mmol, 0.130 g), aldehyde (1.0 mmol), malononitrile (1.0 mmol, 0.066 g), hydrazine hydrate (1.0 mmol, 0.050 g) and Cu-Cytosine@MCM-41 (0.02 g, 2.12 mol%) or Ni-Cytosine@MCM-41 (0.02 g, 0.07 mol%) in water as solvent was stirred in an oil bath at 80 °C for different periods of time (Tables 6 and 7). After completion of the reaction (observed by TLC), the mixture was cooled down to room temperature. Afterwards, the catalyst was separated using simple filtration and, then, washed by hot ethyl acetate. The residue was extracted by ethyl acetate and water. The organic layer was dried over anhydrous sodium sulfate and, then, the solvent was evaporated. The pure product was obtained through recrystallization in ethanol.

2.5 | Selected spectral data

Selected spectral data is given in the Supporting Information.

2.6 | 2-(1H-tetrazol-5-yl)benzonitrile

¹H NMR (400 MHz, DMSO): δ_H = 17.25 (br, 1H), 8.13–8.09 (t, *J* = 8 Hz, 2H), 7.98–7.94 (t, *J* = 8 Hz, 1H), 7.83–7.79 (t, *J* = 8 Hz, 1H) ppm. ¹³C NMR (100 MHz, DMSO): δ_C = 134.9, 133.8, 131.4, 129.7, 127.6, 117.2, 110.2 ppm.

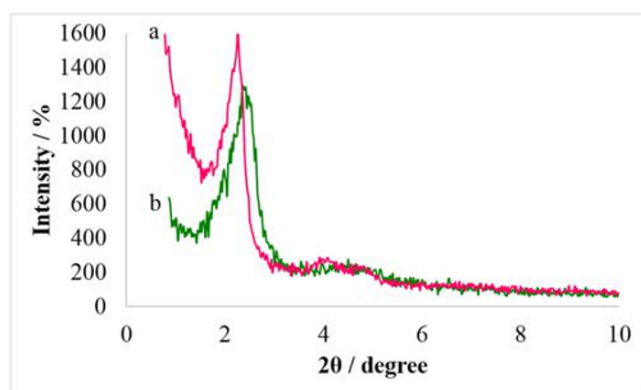


FIGURE 1 The low XRD patterns of Ni-Cytosine@MCM-41 (a) and Cu-Cytosine@MCM-41 (b)

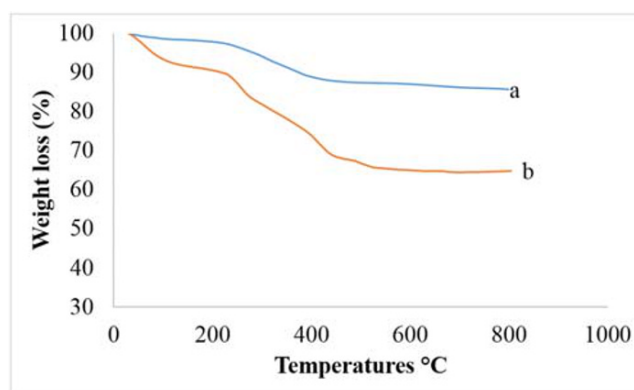


FIGURE 2 TGA diagrams of Cu-Cytosine@MCM-41 (a) and Ni-Cytosine@MCM-41 (b)

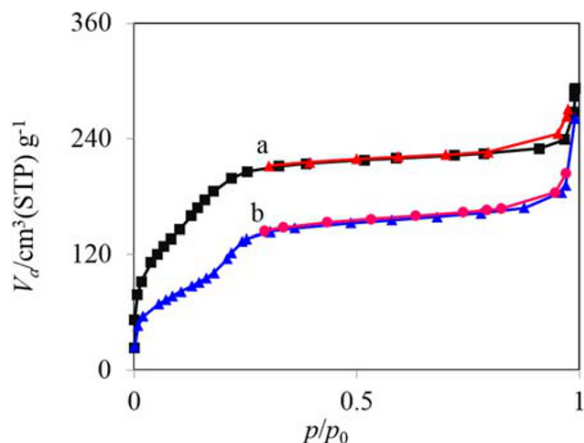


FIGURE 3 N_2 adsorption-desorption isotherms of Cu-Cytosine@MCM-41 (a) and Ni-Cytosine@MCM-41 (b)

2.6.1 | 1-(4-(1H-tetrazol-5-yl)phenyl)ethanone

1H NMR (400 MHz, DMSO): $\delta_H = 17.17$ (br, 1H), 8.22–8.20 (d, $J = 8$ Hz, 2H), 8.19–8.17 (d, $J = 8$ Hz, 2H), 2.67 (s, 3H) ppm. ^{13}C NMR (100 MHz, DMSO): $\delta_C = 212.4$, 151.5, 138.4, 129.2, 128.3, 127.2, 26.9 ppm.

2.6.2 | 6-amino-4-(4-bromophenyl)-3-methyl-2,4-dihydropyrano[2,3-c]pyrazole-5-carbonitrile

1H NMR (400 MHz, DMSO): $\delta_H = 12.16$ (s, 1H), 7.54–7.52 (d, $J = 8$ Hz, 2H), 7.17–7.15 (d, $J = 8$ Hz, 2H), 6.96 (s, 2H), 4.64 (s, 1H), 1.81 (s, 3H) ppm. ^{13}C NMR (100 MHz, DMSO): $\delta_C = 176.9$, 160.9, 143.9, 135.6, 131.3, 129.7, 120.6, 116.7, 97.1, 56.6, 35.6, 9.7 ppm.

2.6.3 | 6-amino-3-methyl-4-(3-nitrophenyl)-2,4-dihydropyrano[2,3-c]pyrazole-5-carbonitrile

1H NMR (400 MHz, DMSO): $\delta_H = 12.23$ (s, 1H), 8.16–8.14 (d, $J = 8$ Hz, 1H), 8.04 (s, 1H), 7.71–7.67 (m, 2H), 7.07 (s, 2H), 4.90 (s, 1H), 1.82 (s, 3H) ppm.

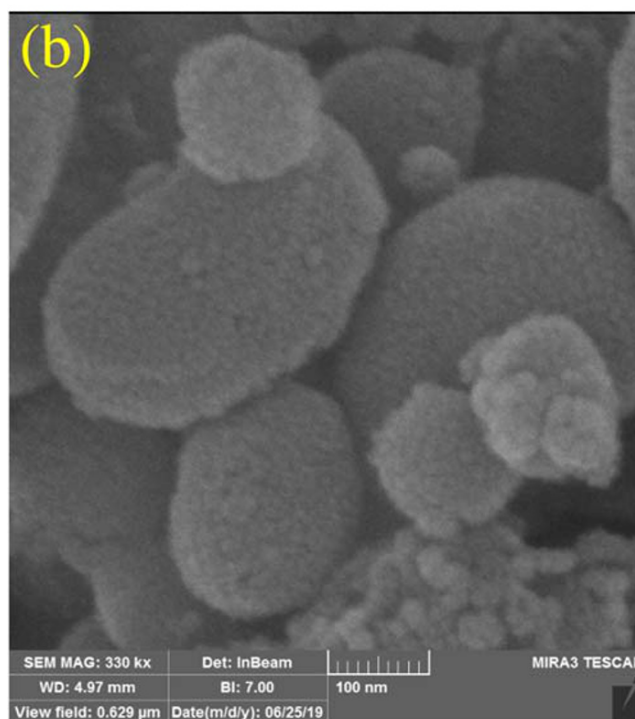
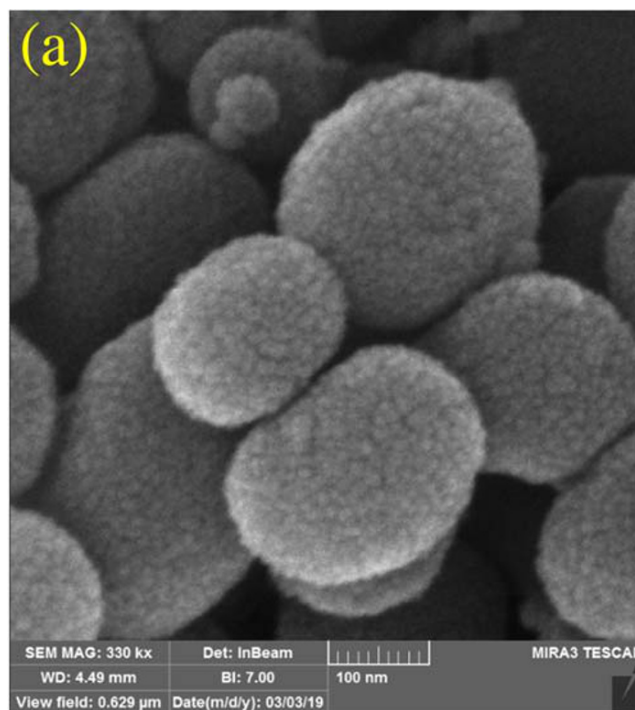


FIGURE 4 SEM images of Cu-Cytosine@MCM-41 (a) and Ni-Cytosine@MCM-41 (b)

TABLE 1 Textural properties of MCM-41, Cu-Cytosine@MCM-41 and Ni-Cytosine@MCM-41

Entry	Sample	S_{BET} (m^2/g)	Pore diameter (nm)	Pore volume ($cm^3 g^{-1}$)
1	MCM-41	1113.7 [74]	2.39 [75]	1.51 [29]
2	Cu-Cytosine@MCM-41	267	0.29	1.29
3	Ni-Cytosine@MCM-41	295	0.35	1.22

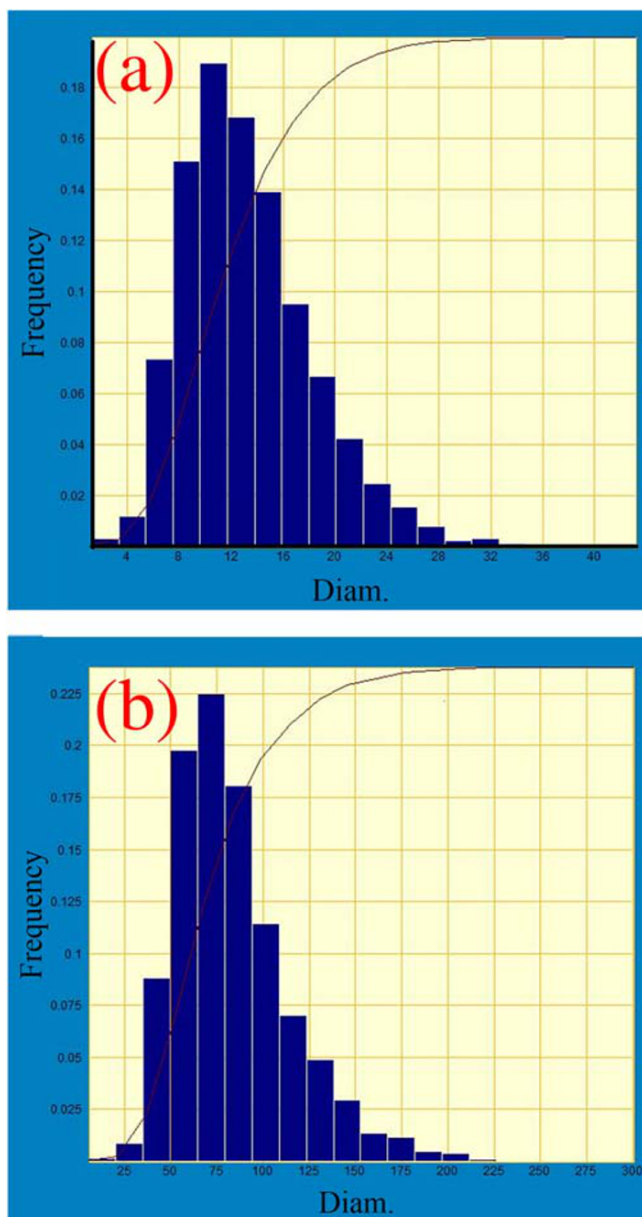


FIGURE 5 Particle size distribution histogram of Cu-Cytosine@MCM-41 (a) and Ni-Cytosine@MCM-41 (b)

2.6.4 | 6-amino-3-methyl-4-(2-nitrophenyl)-2,4-dihydropyrano[2,3-c]pyrazole-5-carbonitrile

^1H NMR (400 MHz, DMSO): δ_{H} = 12.23 (s, 1H), 7.88–7.86 (d, J = 8 Hz, 1H), 7.71–7.67 (t, J = 8 Hz, 1H), 7.53–7.49 (t, J = 8 Hz, 1H), 7.35–7.33 (d, J = 8 Hz, 1H), 7.06 (s, 2H), 5.11 (s, 1H), 1.79 (s, 3H) ppm. ^{13}C NMR (100 MHz, DMSO): δ_{C} = 175.5, 161.1, 149.1, 137.6, 135.6, 133.3, 131.2, 128.3, 123.5, 120.2, 96.3, 56.0, 31.3, 9.5 ppm.

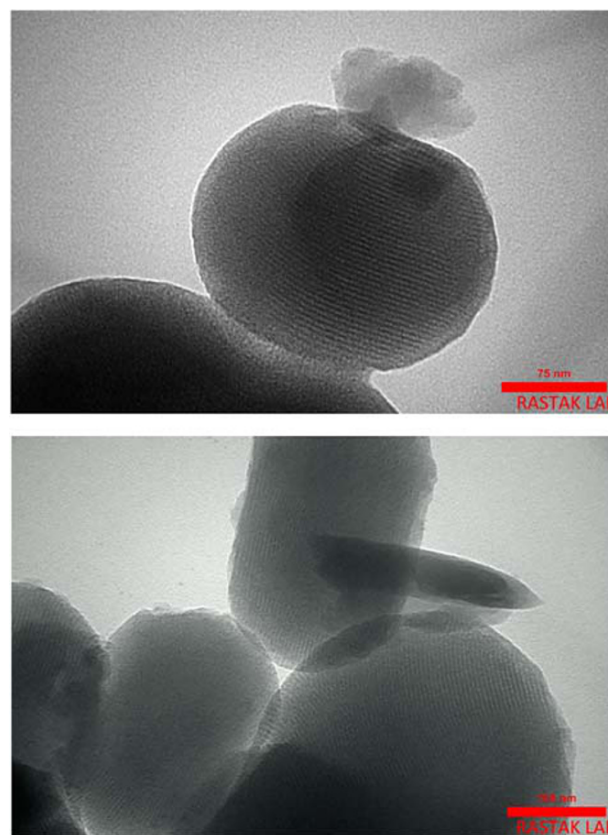


FIGURE 6 TEM images of Cu-Cytosine@MCM-41

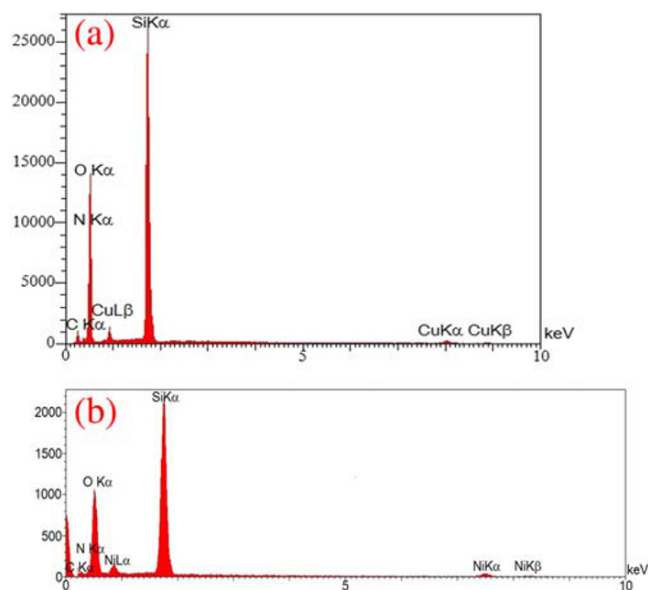


FIGURE 7 EDS diagrams of Cu-Cytosine@MCM-41 (a) and Ni-Cytosine@MCM-41 (b)

3 | RESULTS AND DISCUSSION

The synthesis procedure of Cu-Cytosine@MCM-41 and Ni-Cytosine@MCM-41 is outlined in Scheme 1. Initially, the surface of MCM-41 nanoparticles was modified by

3-chloropropyltrimtoxysilane^[69] and, further cytosine was immobilized on their surface. Subsequently, copper (II) and nickel (II) have been stabilized on Cytosine@MCM-41. Finally, the resulting catalysts were characterized by scanning electron microscopy (SEM), wavelength dispersive X-ray spectroscopy (WDX), energy-dispersive X-ray spectroscopy (EDS), transmission electron Microscopy (TEM), N₂ adsorption–desorption isotherms, thermogravimetric analysis (TGA), Fourier transform infrared spectroscopy (FT-IR), X-ray diffraction (XRD), and atomic absorption spectroscopy (AAS) techniques.

3.1 | Catalyst characterizations

The low angle XRD patterns of Ni-Cytosine@MCM-41 and Cu-Cytosine@MCM-41 are presented in Figure 1. The low angle XRD pattern of Ni-Cytosine@MCM-41 shows several peaks of 2θ value at $2\theta \approx 2.28^\circ$ (1 0 0), $2\theta \approx 4.08^\circ$ (1 1 0) and $2\theta \approx 4.80^\circ$ (2 0 0). Moreover, the low angle XRD pattern of Cu-Cytosine@MCM-41 shows the peaks of 2θ value at $2\theta \approx 2.34^\circ$ (1 0 0), $2\theta \approx 4.12^\circ$ (1 1 0) and $2\theta \approx 4.84^\circ$ (2 0 0). These peaks are due to the hexagonal unit cell of Ni-Cytosine@MCM-41 and Cu-

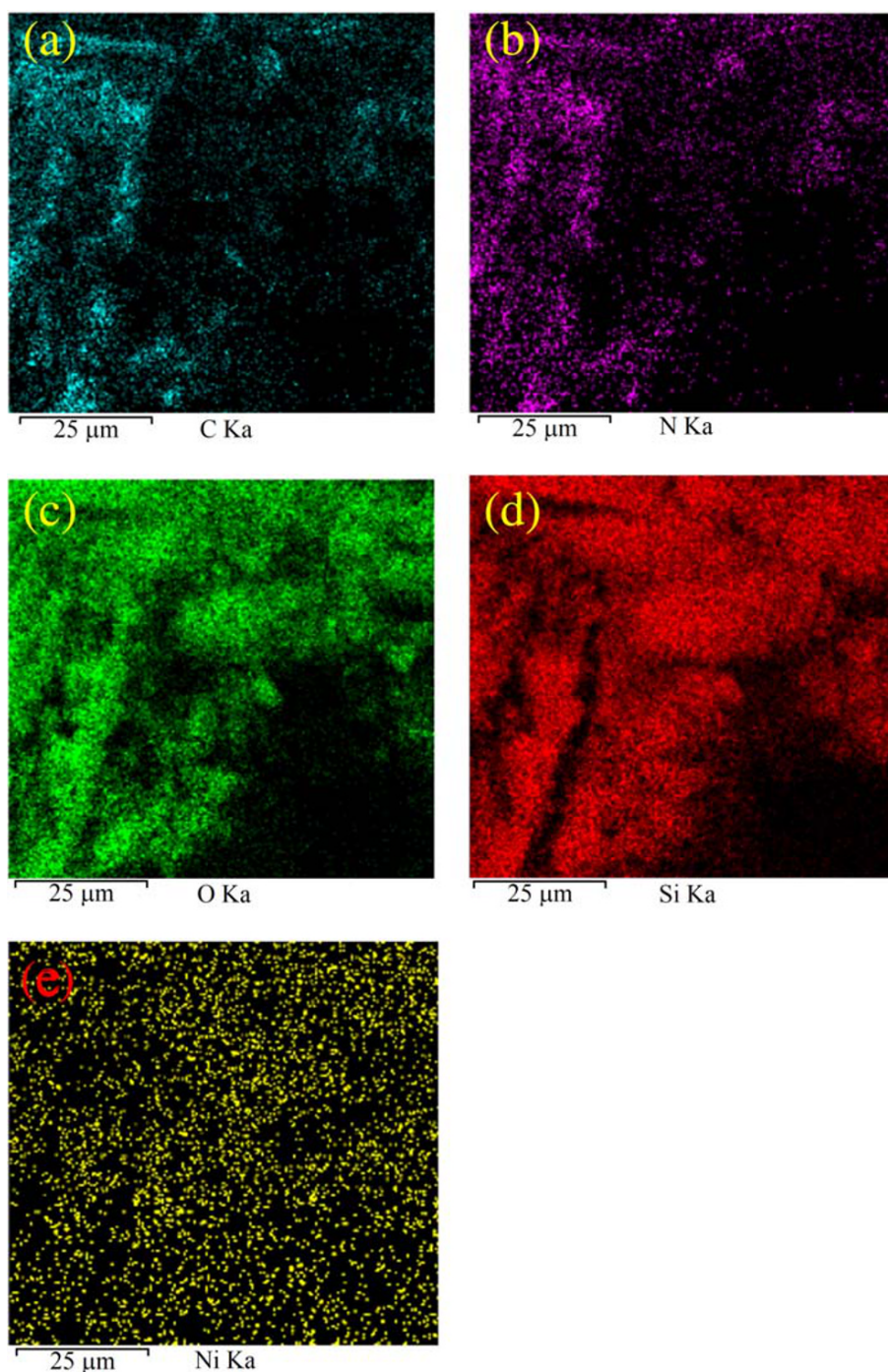
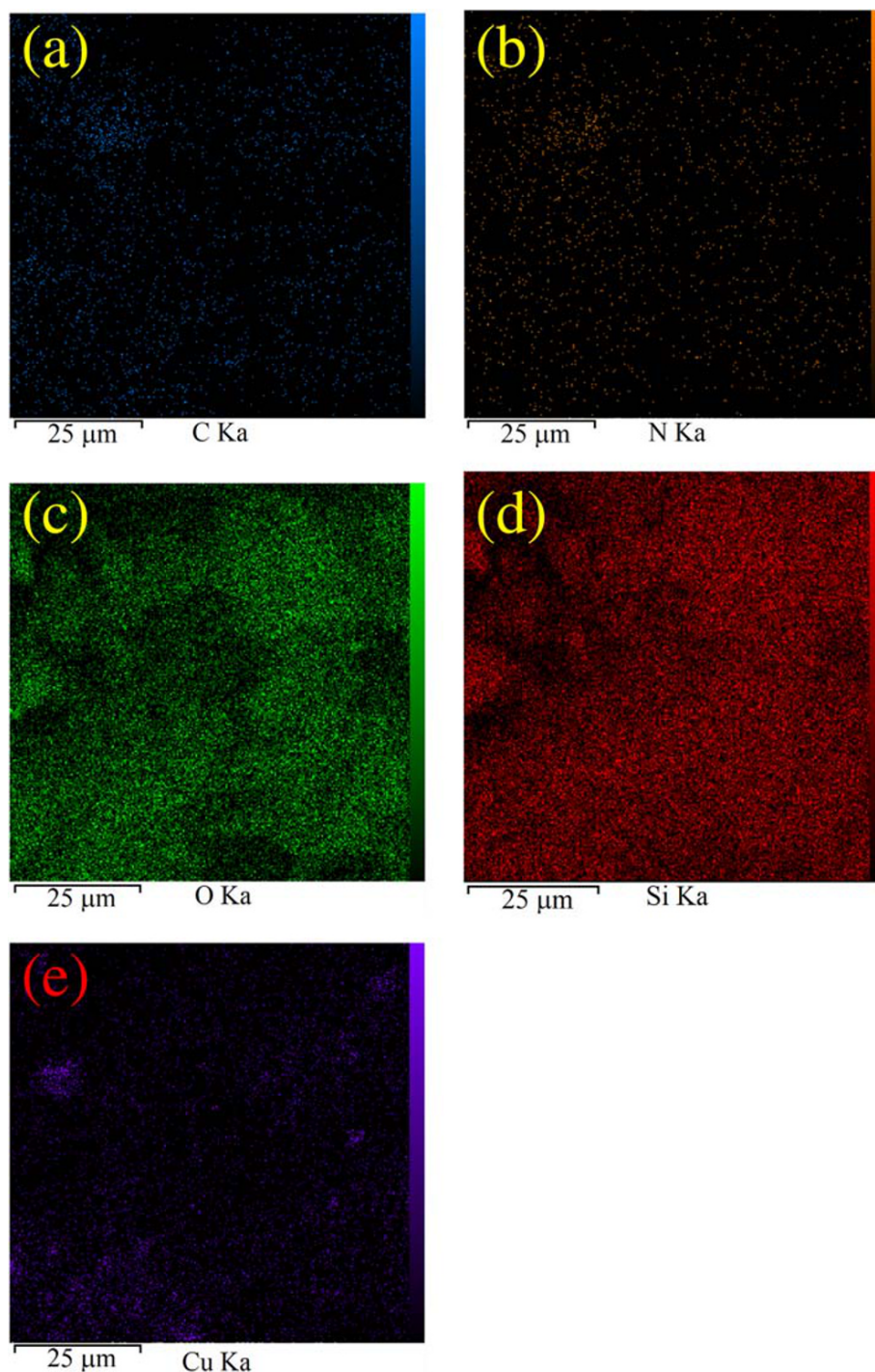


FIGURE 8 Elemental mapping of (a) carbon, (b) nitrogen, (c) oxygen, (d) silica, and (e) nickel for Ni-Cytosine@MCM-41

FIGURE 9 Elemental mapping of (a) carbon, (b) nitrogen, (c) oxygen, (d) silica, and (e) copper for Cu-Cytosine@MCM-41



Cytosine@MCM-41.^[28,69,72] XRD patterns of these catalysts have a sharp (100) peak and two weak peaks (110 and 200) which indicate an ordered hexagonal mesoporous structure of the catalysts. The decreasing intensity of $2\theta \approx 4.12^\circ$ (1 1 0) and $2\theta \approx 4.84^\circ$ (2 0 0) was observed in comparison to the standard XRD pattern of MCM-41 (from 2000 to lower than 1,500^[27,28,69,72]) which is due to the immobilization of the organic layers and metal complex in MCM-41 channels.^[27,28,69,72] These results confirmed that the organic layers were successfully immobilized on MCM-41.

Since a wide range of organic reactions are usually carried out in high temperature, thermal stability of the described catalysts played an important role as confirmed by TGA analysis. The TGA diagrams of Ni-Cytosine@MCM-41 and Cu-Cytosine@MCM-41 are shown in Figure 2. The mass loss is indicated in low temperatures between 25–120 °C, which is 2% and 10% of weight loss for Cu-Cytosine@MCM-41 and Ni-Cytosine@MCM-41, respectively. These mass losses correspond to the removal of solvents.^[73] The second weight loss which is between 240–500 °C is 12% and 26% of

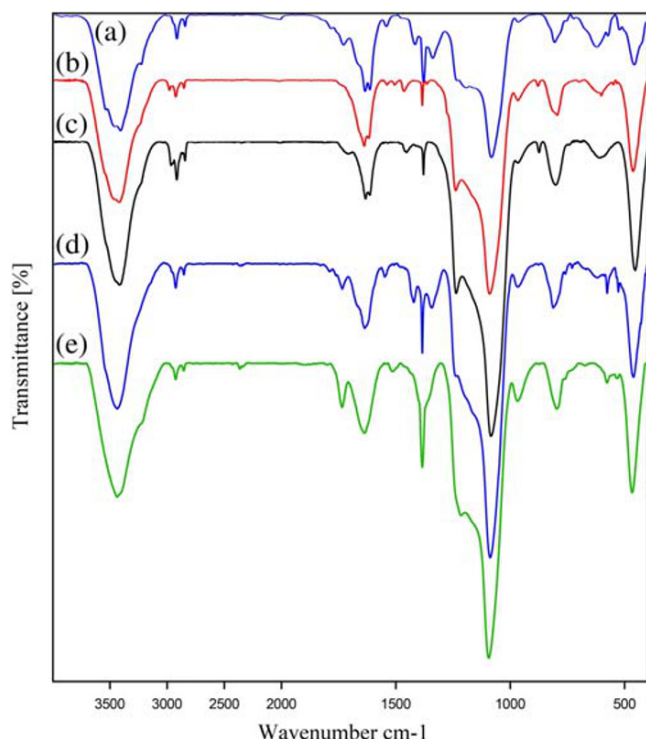
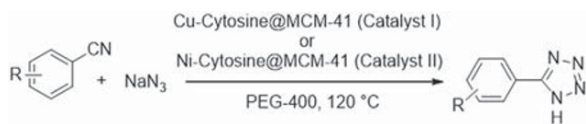


FIGURE 10 FT-IR spectra of MCM-41 (a), CPTMS@MCM-41 (b), Cytosine@MCM-41 (c), Cu-Cytosine@MCM-41 (d) and Ni-Cytosine@MCM-41 (e)

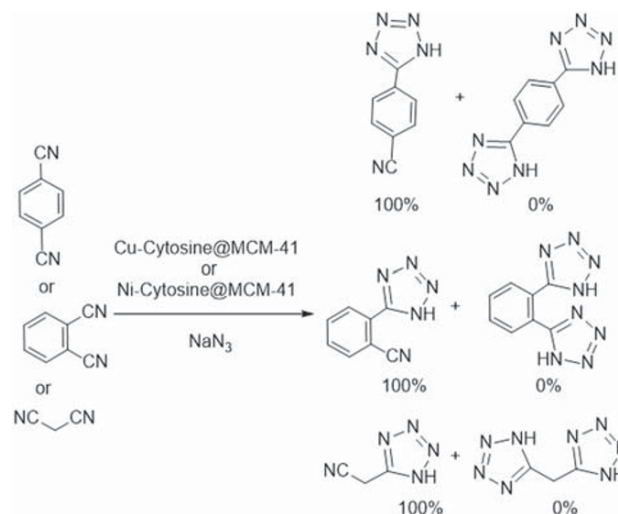


SCHEME 2 Synthesis of 5-substituted 1H-tetrazoles in the presence of Cu-Cytosine@MCM-41 or Ni-Cytosine@MCM-41

the weight loss for Cu-Cytosine@MCM-41 and Ni-Cytosine@MCM-41, respectively. These mass losses are related to the calcination of organic groups which were immobilized on MCM-41 nanoparticles.^[61] The final mass loss which was a small weight loss above 600 °C (lower than 3%) may be related to the condensation of the silanol groups on MCM-41.^[27]

Based on TGA diagrams of Ni-Cytosine@MCM-41 and Cu-Cytosine@MCM-41, no weight loss was seen up to 230 °C (except for the evaporated solvents) indicating that these catalysts are stable even at 230 °C. The results confirmed that the cytosine complexes of copper and nickel are covalently immobilized on MCM-41 nanoparticles.

Nitrogen adsorption-desorption isotherms of Ni-Cytosine@MCM-41 and Cu-Cytosine@MCM-41 are shown in Figure 3. Besides, the obtained results from these analyses are summarized in Table 1. Figure 3 displayed type IV of IUPAC classification, which is in accordance to mesoporous material.^[29] Based on



SCHEME 3 Homoselectivity of Cu-Cytosine@MCM-41 or Ni-Cytosine@MCM-41 in [3 + 2] cycloaddition of NaN_3 with dicyano substituted derivatives

Brunauer-Emmett-Teller (BET), the surface areas of Ni-Cytosine@MCM-41 and Cu-Cytosine@MCM-41 are 295 and 267 m^2/g , respectively. The BET surface area of these catalysts is lower than mesoporous MCM-41 (1113.7 m^2/g ^[74]) which is due to the immobilization of organic groups and metal complexes into channels of MCM-41 nanoparticles. The pore volumes of Ni-Cytosine@MCM-41 and Cu-Cytosine@MCM-41 are 0.35 cm^3g^{-1} and 0.29 cm^3g^{-1} , respectively, which are lower than the pore volume of MCM-41 (1.51 cm^3g^{-1} ^[29]). Besides, the pore diameters of Ni-Cytosine@MCM-41 and Cu-Cytosine@MCM-41 are 1.22 and 1.29 nm, respectively which are lower than MCM-41 (2.39 nm^[75]). Decreases in surface area, pore volumes and pore diameters of Ni-Cytosine@MCM-41 and Cu-Cytosine@MCM-41 are due to the grafting of organic layers and metal complexes into channels of MCM-41.^[27]

The particles size and shape of Cu-Cytosine@MCM-41 and Ni-Cytosine@MCM-41 were studied by SEM technique. SEM images of these catalysts are shown in Figure 4. Nearly spherical nanoparticles of this catalyst are clearly indicated in SEM images. In order to indicate the particle size distribution of these catalysts, the histogram of particles size which have been obtained from SEM images are shown in Figure 5. As shown, the particles size of Cu-Cytosine@MCM-41 and Ni-Cytosine@MCM-41 show homogeneous diameters in the obtained histogram SEM images. As shown, The TEM images showed a good stable morphology of MCM-41 after post-modifications (Figure 6). The uniform size, quasi-spherical morphology and the ordered hexagonal mesoporous structure of the catalysts (less than 5 nm) have been clearly indicated in TEM images.

TABLE 2 Optimization reaction conditions for the synthesis of tetrazoles in the presence of Cu-Cytosine@MCM-41 or Ni-Cytosine@MCM-41

Entry	Catalyst	Amount of catalyst (mg)	Solvent	NaN ₃ (mmol)	Temperature (°C)	Time (min)	Yield (%) ^a
1	Catalyst I	10	PEG	1.3	120	115	64
2	Catalyst I	20	PEG	1.3	120	75	73
3	Catalyst I	30	PEG	1.3	120	30	96
4	Catalyst I	40	PEG	1.3	120	25	96
5	Catalyst I	30	H ₂ O	1.3	100	65	81
6	Catalyst I	30	DMSO	1.3	120	480	71
7	Catalyst I	30	DMF	1.3	120	210	52
8	Catalyst I	30	n-hexane	1.3	Reflux	150	Trace
9	Catalyst I	30	PEG	1.3	100	80	91
10	Catalyst I	30	PEG	1.5	120	30	90
11	Catalyst II	20	PEG	1.3	120	180	91
12	Catalyst II	30	PEG	1.3	120	60	92
13	Catalyst II	30	H ₂ O	1.3	100	196	85
14	Catalyst II	30	DMSO	1.3	120	280	88
15	Catalyst II	30	DMF	1.3	120	540	64
16	Catalyst II	30	PEG	1.2	120	180	90
17	Catalyst II	30	PEG	1.3	100	240	90

^aIsolated yield, ^bNo reaction.

TABLE 3 The role of Cu-Cytosine@MCM-41 and Ni-Cytosine@MCM-41 in the synthesis of tetrazoles in comparison of nickel nitrate, copper nitrate, MCM-41 and cytosine as catalyst under optimized conditions

Entry	Nitrile	Catalyst	Time (min)	Yield (%)
1	Benzonitrile	MCM-41	410	61
2	Benzonitrile	Cytosine	375	64
3	Benzonitrile	Nickel nitrate	60	89
4	Benzonitrile	Copper nitrate	30	91
5	Benzonitrile	Cu-Cytosine@MCM-41	30	96
6	Benzonitrile	Ni-Cytosine@MCM-41	60	92

The element's content of Cu-Cytosine@MCM-41 and Ni-Cytosine@MCM-41 was determined using EDS analysis. The EDS diagrams of these catalysts are shown in Figure 7. As depicted, the EDS result of Cu-Cytosine@MCM-41 shows the presence of silica, oxygen, carbon, nitrogen and also copper species. Moreover, the EDS result of Ni-Cytosine@MCM-41 shows the presence of silica, oxygen, carbon, nitrogen and also nickel species.

X-Ray Mapping (WDX) is an analytical tool used to non-destructively determine the elemental analysis and chemical composition of the samples. In this analysis, a little amount of the sample is bombarded using an electron beam. In this sense, the emitted x-rays wavelengths were the characteristics of the elements. This analysis can be applied for the distributions of elements in materials.

The EDS analyses of Cu-Cytosine@MCM-41 and Ni-Cytosine@MCM-41 were confirmed by X-Ray Mapping (WDX) which is shown in Figures 8 and 9. The WDX analyses exhibit a homogeneous distribution of elements' content in the structure of Cu-Cytosine@MCM-41 and Ni-Cytosine@MCM-41.

In addition, AAS technique was applied to measure the exact amount of copper or nickel in the described catalysts. The exact amount of copper in Cu-Cytosine@MCM-41 was found to be $1.06 \times 10^{-3} \text{ mol g}^{-1}$. Based on obtained results from AAS analysis, the exact amount of nickel in Ni-Cytosine@MCM-41 was found to be $0.034 \times 10^{-3} \text{ mol g}^{-1}$.

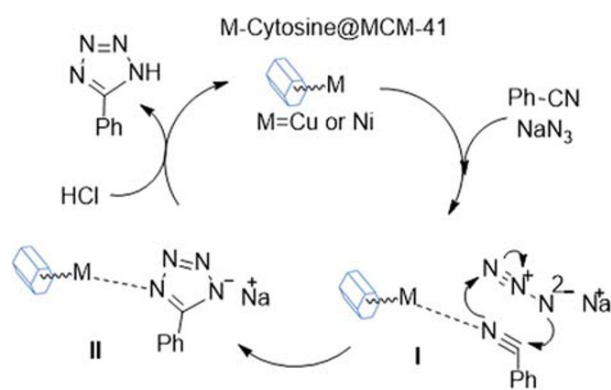
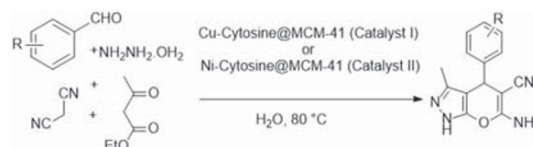
The FT-IR spectra of MCM-41, CPTMS@MCM-41, Cytosine@MCM-41, Cu-Cytosine@MCM-41 and Ni-

TABLE 4 Synthesis of tetrazoles in the presence of Cu-Cytosine@MCM-41

Entry	Nitrile	Time (min)	TOF (h ⁻¹)	Yield ^a (%)	Melting point (°C)	Reported melting point (°C)
1	Benzonitrile	30	61.9	96	211–213	212–214 [64]
2	4-Hydroxybenzonitrile	120	15.5	96	229–231	231–234 [64]
3	4-Nitrobenzonitrile	30	60.6	94	216–218	217–220 [61]
4	2-Chlorobenzonitrile	60	29.3	91	180–183	180–183 [61]
5	4-Chlorobenzonitrile	30	61.9	96	261–263	261–263 [61]
6	3-Chlorobenzonitrile	15	125.2	97	132–134	128–130 [59]
7	3-Nitrobenzonitrile	30	60.0	93	148–150	149–152 [61]
8	4-Acetylbenzonitrile	90	19.3	90	171–173	173–176 [61]
9	Phthalonitrile	15	117.4	91	208–210	209–210 [69]
10	Terephthalonitrile	15	122.6	95	250	250–254 [64]
11	4-Bromobenzonitrile	105	15.8	86	259–261	265–268 [59]
12	Malononitrile	15	121.3	94	114–116	114–116 [69]

^aIsolated yield.**TABLE 5** Synthesis of tetrazoles in the presence of Ni-Cytosine@MCM-41

Entry	Nitrile	Time (min)	TOF (h ⁻¹)	Yield ^a (%)	Melting point (°C)	Reported melting point (°C)
1	Benzonitrile	60	920	92	211–213	213–214 [59]
2	4-Hydroxybenzonitrile	30	1940	97	229–231	231–233 [69]
3	4-Nitrobenzonitrile	90	620	93	216–218	217–220 [61]
4	2-Chlorobenzonitrile	60	940	94	180–182	180–183 [61]
5	3-Chlorobenzonitrile	140	385.7	90	131–133	128–130 [59]
6	3-Nitrobenzonitrile	240	232.5	93	148–150	149–152 [61]
7	4-Acetylbenzonitrile	90	606.7	91	172–174	173–176 [61]
8	Phthalonitrile	60	900	90	209–211	209–210 [69]
9	Terephthalonitrile	60	920	92	251	250–254 [64]
10	2-Hydroxybenzonitrile	60	950	95	223–225	224–226 [61]
11	Malononitrile	30	1920	96	113–115	114–116 [59]

^aIsolated yield.**SCHEME 4** A cyclic mechanism for the synthesis of tetrazoles in the presence of Cu-Cytosine@MCM-41 or Ni-Cytosine@MCM-41**SCHEME 5** Synthesis of pyranopyrazoles in the presence of Cu-Cytosine@MCM-41 or Ni-Cytosine@MCM-41

Cytosine@MCM-41 are indicated in Figure 10. In the FT-IR spectrum of mesoporous MCM-41, three peaks at 463, 811, and 1,075 cm⁻¹ correspond to the Si–O–Si vibrations.^[27] Stretching vibration of surface O–H bonds is indicated at 3417 cm⁻¹. Besides, stretching vibrational modes at 2924 and 2,853 cm⁻¹ in the FT-IR spectrum of CPTMS@MCM-41 are related to the C–H bonds.^[18]

TABLE 6 Optimization reaction conditions for the synthesis of pyranopyrazoles in the presence of Cu-Cytosine@MCM-41 or Ni-Cytosine@MCM-41

Entry	Catalyst	Amount of catalyst (mg)	Solvent	Temperature (°C)	Time (min)	Yield (%) ^a
1	Catalyst I	15	Ethanol	80	600	22
2	Catalyst I	20	Ethanol	80	140	71
3	Catalyst I	20	PEG	80	600	31
4	Catalyst I	15	H ₂ O	80	225	90
5	Catalyst I	20	H ₂ O	80	120	95
6	Catalyst I	25	H ₂ O	80	110	96
7	Catalyst I	20	H ₂ O	60	180	92
8	Catalyst I	20	H ₂ O	40	420	88
9	Catalyst II	15	H ₂ O	80	120	91
10	Catalyst II	20	H ₂ O	80	45	94
11	Catalyst II	25	H ₂ O	80	40	96
12	Catalyst II	20	PEG	80	540	44
13	Catalyst II	20	Ethanol	80	240	41
14	Catalyst II	20	DMSO	80	540	23
15	Catalyst II	20	DMF	80	360	40
16	Catalyst II	20	H ₂ O	60	85	90
17	Catalyst II	20	H ₂ O	40	125	83

^aIsolated yield.**TABLE 7** Synthesis of pyranopyrazoles in the presence of Cu-Cytosine@MCM-41

Entry	Aldehyde	Time (min)	TOF (h ⁻¹)	Yield ^a (%)	Melting point (°C)	Reported melting point (°C)
1	4-Chlorobenzaldehyde	120	22.4	95	233–236	232–233 [70]
2	3-Nitrobenzaldehyde	75	34.3	91	243–245	243–245 [53]
3	3-Hydroxybenzaldehyde	55	48.4	94	232–241	241–242 [71]
4	4-Hydroxybenzaldehyde	35	72.8	90	220–222	222–224 [55]
5	4-Bromobenzaldehyde	30	87.7	93	181–183	183–185 [53]
6	3,4-Dimethoxybenzaldehyde	36	73.1	93	190–192	192–194 [54]
7	Benzaldehyde	60	42.4	90	242–246	244–246 [54]
8	2-Nitrobenzaldehyde	65	40.9	94	218–220	220–222 [54]
9	4-Methoxybenzaldehyde	15	179.2	95	208–210	209–211 [53]
10	4-Methylbenzaldehyde	15	175.5	93	203–206	221–22 [70]
11	4-Fluorobenzaldehyde	30	84.9	90	169–172	170–172 [54]

^aIsolated yield.

Several peaks at 1619, 1457, 1,384, 1,241, 996, 878, and 794 cm⁻¹ in the FT-IR spectrum of Cytosine@MCM-41 confirm that cytosine was successfully immobilized on MCM-41.

3.2 | Catalytic study

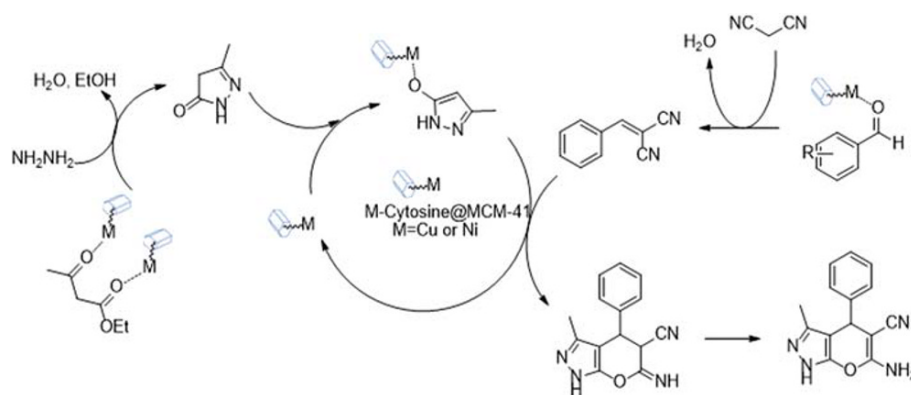
Catalytic activities of Cu-Cytosine@MCM-41 and Ni-Cytosine@MCM-41 were studied in the synthesis of 5-

substituted 1H-tetrazoles (Scheme 2) and pyranopyrazoles (Scheme 3).

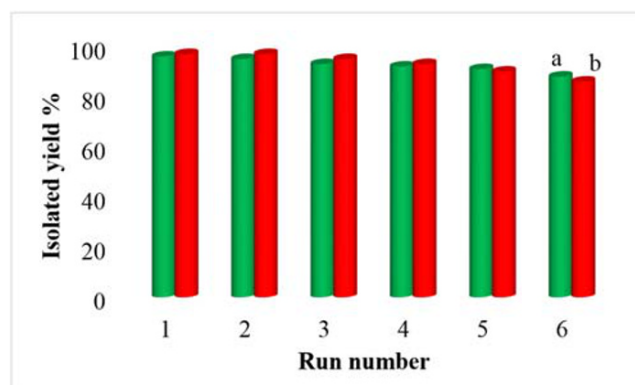
To optimize the reaction conditions for the synthesis of 5-substituted 1H-tetrazoles, various parameters such as the amount of catalysts, different solvents, various concentrations of sodium azide and temperature were examined in the [3 + 2] cycloaddition of sodium azide and benzonitrile as the model reaction (Table 2). Based on the outlined results in Table 2, the best results were obtained in the presence of 30 mg (3.1 mol%) of Cu-

TABLE 8 Synthesis of pyranopyrazoles in the presence of Ni-Cytosine@MCM-41

Entry	Aldehyde	Time (min)	TOF (h^{-1})	Yield ^a (%)	Melting point ($^{\circ}\text{C}$)	Reported melting point ($^{\circ}\text{C}$)
1	4-Chlorobenzaldehyde	45	1790.5	94	232–236	232–233 [70]
2	3-Nitrobenzaldehyde	100	771.4	90	231–234	233–235 [55]
3	3-Hydroxybenzaldehyde	110	709.1	91	232–241	241–242 [71]
4	4-Hydroxybenzaldehyde	140	557.1	91	219–221	222–224 [54]
5	4-Bromobenzaldehyde	135	571.4	90	173–175	183–185 [53]
6	3,4-Dimethoxybenzaldehyde	110	732.5	94	195–196	192–194 [54]
7	5-bromo-2-hydroxybenzaldehyde	205	376.3	90	224–226	226–227 [70]
8	2-Nitrobenzaldehyde	125	603.4	88	220–222	220–222 [54]
9	4-Methoxybenzaldehyde	30	2685.7	94	210–211	209–211 [53]
10	4-Methylbenzaldehyde	25	3,120	91	203–206	221–222 [70]
11	4-Fluorobenzaldehyde	60	1,300	91	168–170	170–172 [54]

^aIsolated yield.**SCHEME 6** A cyclic mechanism for the synthesis of pyranopyrazoles in the presence of Cu-Cytosine@MCM-41 or Ni-Cytosine@MCM-41

Cytosine@MCM-41 (Table 2, entry 3) or 30 mg (0.1 mol%) of Ni-Cytosine@MCM-41 (Table 2, entry 12) in PEG-400 as the green solvent at 120 $^{\circ}\text{C}$ using 1.3 mmol of sodium azide. When the model reaction was repeated at 100 $^{\circ}\text{C}$ (Table 2, entries 8, 17), the product yields were decreased to 91% and 90% at longer times in the presence of Cu-Cytosine@MCM-41 and Ni-Cytosine@MCM-41, respectively. Moreover, the lower amounts of Cu-Cytosine@MCM-41 (20 mg) and Ni-Cytosine@MCM-41 (20 mg) gave a lower yield of the products in longer times (Table 2, entries 2 and 11). Besides, various polar solvents such as H_2O , dimethyl sulfoxide (DMSO), dimethylformamide (DMF) and PEG-400 have been examined to obtain the best reaction conditions. In addition, the effect of nonpolar solvents such as n-hexane was examined in the model reaction (Table 2, entry 8) in which unsuitable results were obtained. The best results were obtained in PEG-400 (Table 2, entries 3 and 11). The effect of sodium azide concentration was also studied and, consequently, the best results were obtained using 1.3 mmol of sodium azide.

**FIGURE 11** Reusability of the Cu-Cytosine@MCM-41 (a) and Ni-Cytosine@MCM-41 (b) in the synthesis of 4-(1H-tetrazol-5-yl)phenol

In order to show the role of Cu-Cytosine@MCM-41 and Ni-Cytosine@MCM-41 in the synthesis of tetrazoles, the model reaction has been examined in the presence of a catalytic amount of nickel nitrate, copper nitrate,

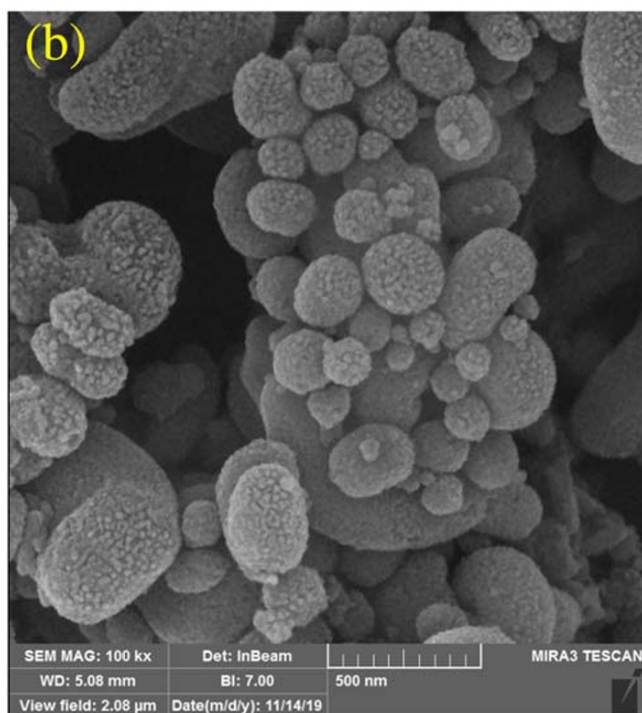
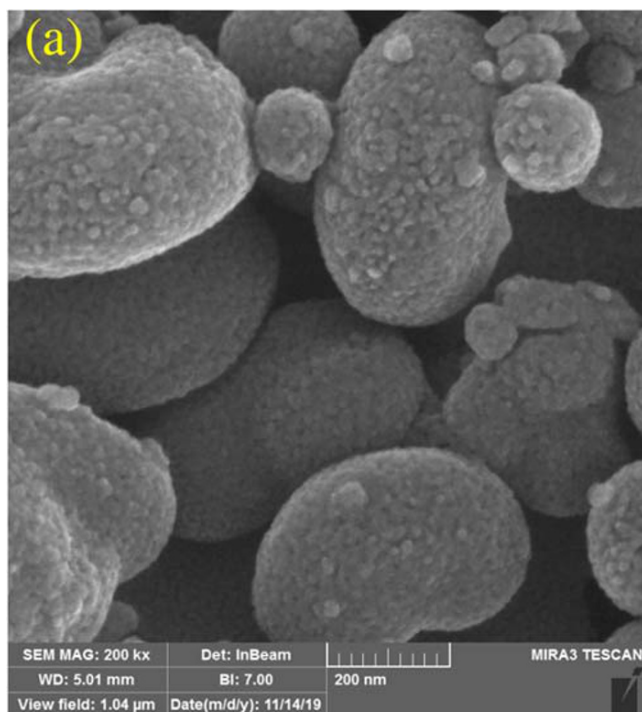


FIGURE 12 SEM images of Cu-Cytosine@MCM-41 (a) and Ni-Cytosine@MCM-41 (b) after recycling

MCM-41 and cytosine as catalyst. Besides, the obtained results were compared those of the Ni-Cytosine@MCM-41 and Ni-Cytosine@MCM-41 (Table 3). As shown in Table 3, the reaction was not completed in the presence of MCM-41 (Table 3, entry 1) or cytosine (Table 3, entry

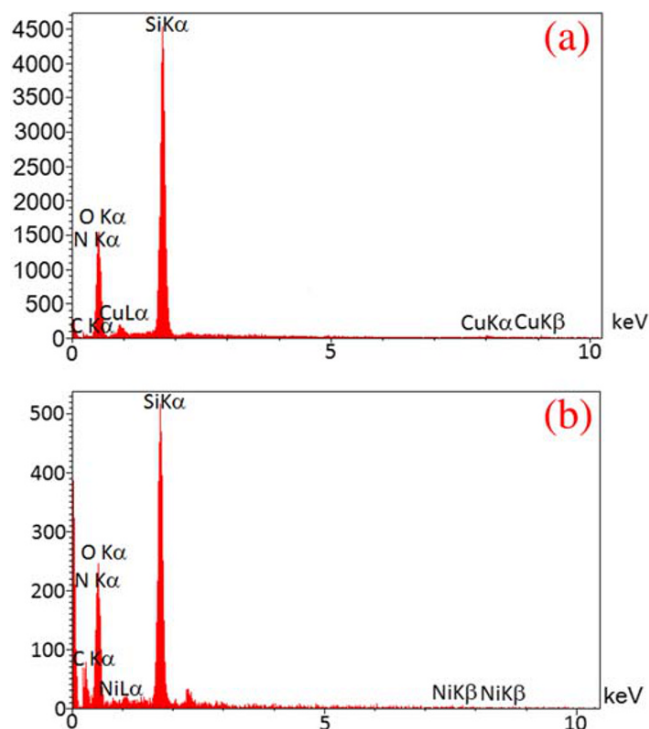


FIGURE 13 EDS diagrams of recovered Cu-Cytosine@MCM-41 (a) and recovered Ni-Cytosine@MCM-41 (b)

2) even when the reaction time is extended. In this sense, Ni-Cytosine@MCM-41 and Cu-Cytosine@MCM-41 are comparable to the homogeneous nickel (Table 3, entry 3) and copper (Table 3, entry 4) in terms of the reaction times and the isolated yields. That is because high surface area is available due to high porosity of these catalysts.

The catalytic activity of Cu-Cytosine@MCM-41 and Ni-Cytosine@MCM-41 was explored in [3 + 2] cycloaddition of sodium azide (NaN_3) with several benzonitrile derivatives bearing electron-donating or electron-withdrawing groups. The obtained results are summarized in Tables 4 and 5. As shown in Table 4, all of the products were obtained in high yields and high TOF values indicating the high efficiency of Cu-Cytosine@MCM-41 (Table 4) and Ni-Cytosine@MCM-41 (Table 5) in the synthesis of tetrazoles.

Homoselectivity is an interesting property of some organic reactions which can be observed in the same functional groups.^[76] The homoselectivity of Cu-Cytosine@MCM-41 and Ni-Cytosine@MCM-41 was studied in the [3 + 2] cycloaddition of NaN_3 with phthalonitrile, terephthalonitrile and malononitrile; possessing two cyano functional groups with same position in its structure. Interestingly, these procedures illustrated a good homoselectivity and afforded the mono-addition products in the presence of these catalysts (Scheme 4).

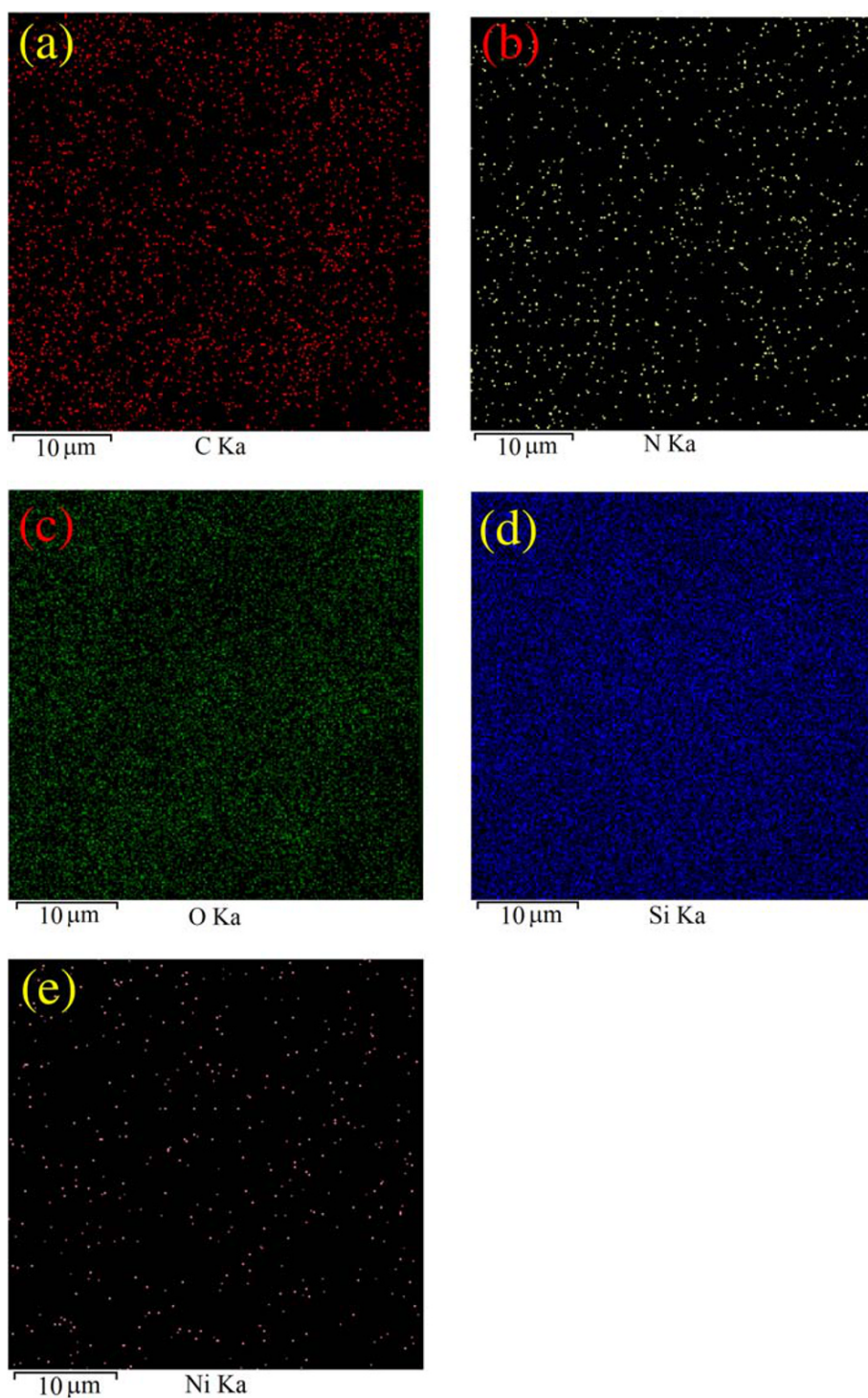


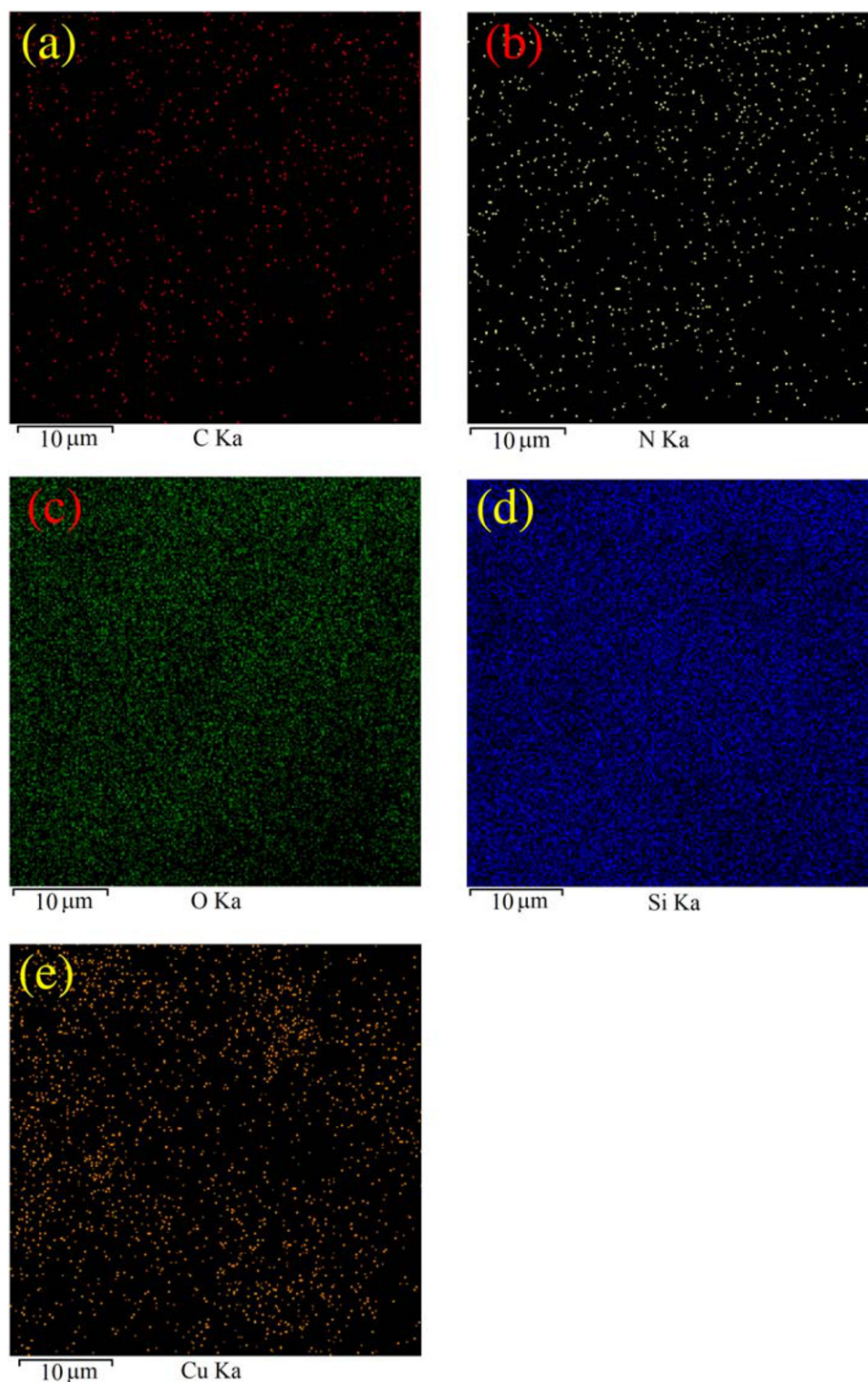
FIGURE 14 Elemental mapping of (a) C, (b) N, (c) O, (d) Si, and (e) Ni for Ni-Cytosine@MCM-41

Based on previously reported, a mechanism for the synthesis of tetrazoles is outlined in Scheme 4 in the presence of Cu-Cytosine@MCM-41 or Ni-Cytosine@MCM-41.^[61,64]

In continuation, the synthesis of pyranopyrazoles was studied in the presence of Cu-Cytosine@MCM-41 and Ni-Cytosine@MCM-41 which is outline in Scheme 5.

In order to optimize the reaction conditions for the synthesis of pyranopyrazoles, various parameters such as the amount of catalysts, different solvents and temperature were examined in the four-component condensation of ethyl acetoacetate, 4-chloroaldehyde, malononitrile, and hydrazine hydrate as the model reaction. The results of these studies are summarized in Table 6 in which the best results were obtained

FIGURE 15 Elemental mapping of (a) C, (b) N, (c) O, (d) Si, and (e) Cu for Cu-Cytosine@MCM-41 (b)



in the presence of 20 mg (2.12 mol%) of Cu-Cytosine@MCM-41 (Table 6, entry 5) or 20 mg (0.07 mol%) of Ni-Cytosine@MCM-41 (Table 6, entry 10) in water at 80 °C.

The scope catalytic activity of Cu-Cytosine@MCM-41 and Ni-Cytosine@MCM-41 was explored in the multicomponent reaction of various aldehyde with ethyl acetoacetate, malononitrile, and hydrazine hydrate under optimized conditions. A wide range of

aromatic aldehydes bearing electron-donating or electron-withdrawing groups were investigated to synthesize the corresponding pyranopyrazole derivatives. All of the pyranopyrazoles were obtained in high yields. Moreover, TOF values indicated the high efficiency of Cu-Cytosine@MCM-41 (Table 7) and Ni-Cytosine@MCM-41 (Table 8) in the synthesis of pyranopyrazole. The obtained results are presented in Tables 7 and 8.

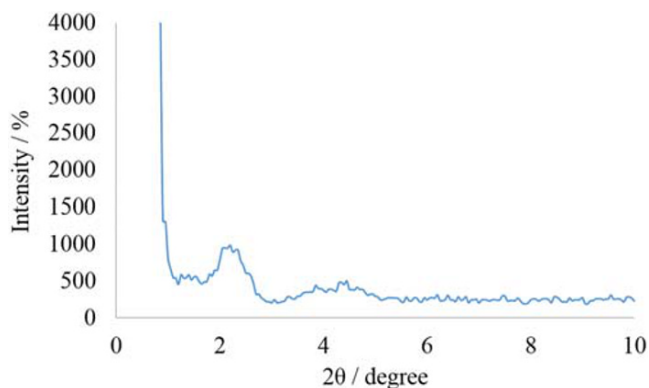


FIGURE 16 The low angle XRD patterns of Cu-Cytosine@MCM-41 after recycling

Based on previously reported, a mechanism for the synthesis of pyranopyrazoles is outlined in Scheme 6 in the presence of Cu-Cytosine@MCM-41 or Ni-Cytosine@MCM-41.^[51]

3.3 | Catalysts recovery

In this study, we investigated the recoverability and recyclability of the Cu-Cytosine@MCM-41 and Ni-Cytosine@MCM-41 in the synthesis of 4-(1H-tetrazol-5-yl)phenol ([2 + 3] cycloaddition reaction of 4-hydroxybenzotrile with sodium azide. In this sense, after completion of the reaction, the catalyst was

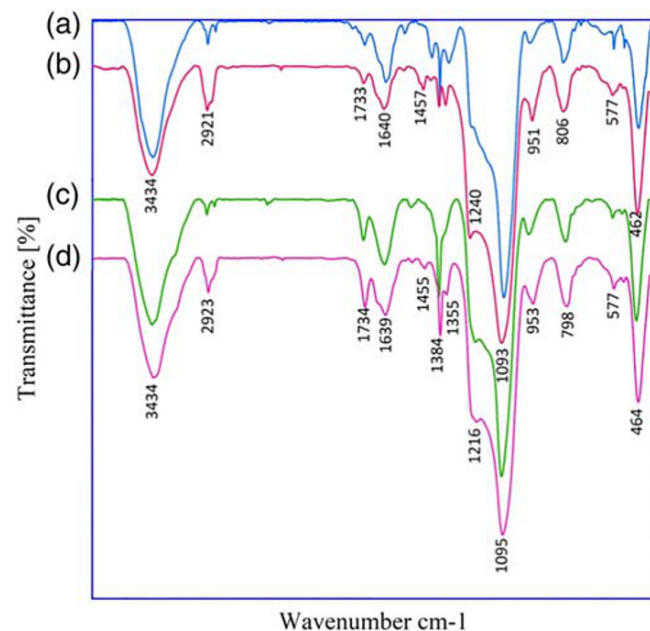


FIGURE 17 FT-IR spectra of Cu-Cytosine@MCM-41 (a), recovered Cu-Cytosine@MCM-41 (b), Ni-Cytosine@MCM-41 (c), and recovered Ni-Cytosine@MCM-41 (d)

recovered by centrifugation and, then, reused in the next run up to 6 times. The results of these studied are presented in Figure 11.

3.4 | Characterization of recycled catalysts

In order to indicate the stability of the described catalysts in this work, the nanocatalysts were characterized by SEM, EDS, WDX, XRD, FT-IR and AAS techniques before and after reusing.

After being reused, the particle sizes of Cu-Cytosine@MCM-41 and Ni-Cytosine@MCM-41 were compared to the fresh catalysts (Figure 12). As shown, the size and morphology of the recycled catalysts indicated an excellent similarity to the fresh catalysts.

The elements content of Cu-Cytosine@MCM-41 and Ni-Cytosine@MCM-41 was described using EDS analysis which shows the presence of Si, O, C, N and Cu species in Cu-Cytosine@MCM-41 (Figure 13). Moreover, Si, O, C, N and Ni species were observed in the EDS analyses of Ni-Cytosine@MCM-41 (Figure 13). The distributions of elements content of these catalysts were observed by WDX which exhibits homogeneous distributions of elements content in the structure of Cu-Cytosine@MCM-41 (Figures 14) and Ni-Cytosine@MCM-41 (Figures 15).

The low angle XRD pattern of the recovered Cu-Cytosine@MCM-41 which is shown in Figure 16 includes several peaks at $2\theta \approx 2.35^\circ$, $2\theta \approx 3.95^\circ$ and $2\theta \approx 4.75^\circ$. Similar to the fresh catalyst, these peaks exhibit the hexagonal unit cell of Cu-Cytosine@MCM-41. Therefore, the XRD pattern of the recovered catalyst showed good stability of the catalyst after recycling. Based on the information obtained from the XRD pattern of the recovered Cu-Cytosine@MCM-41, it is clear that the crystalline structure and hexagonal unit cell of this catalyst has not been changed after recycling.

The FT-IR spectra of the recovered catalysts were compared to the fresh catalysts (Figure 17) in which no change was observed in FT-IR spectra after recovering. These results are good witnesses for the stability of Cu-Cytosine@MCM-41 and Ni-Cytosine@MCM-41 under the reaction conditions. Therefore, these catalysts can be recovered and reused for several runs without any change in their structure.

3.5 | Leaching study of the catalysts

Metal leaching of Cu-Cytosine@MCM-41 and Ni-Cytosine@MCM-41 was studied by AAS analysis. In this regard, [2 + 3] cycloaddition of benzonitrile with

TABLE 9 Comparison of Cu-Cytosine@MCM-41 and Ni-Cytosine@MCM-41 in the synthesis of 5-phenyl-1H-tetrazole with previously reported procedures

Entry	Catalyst	Condition	Time (hr)	Yield (%)	TOF (h ⁻¹)	Ref.
1	(NH ₄)Ce(NO ₃) ₆	DMF, 110 °C	6	97	1.61	[77]
2	Sm@I-MSN	DMF, 100 °C	5	87	40.7	[60]
3	Fe ₃ O ₄ @SiO ₂ /Salen Cu (II)	DMF, 120 °C	7	90	-	[78]
4	ammonium chloride and ammonium fluoride	DPOL/H ₂ O (6/4), 160 °C	48	95	0.10	[79]
5	AgNO ₃	DMF, 120 °C	5	83	1.66	[80]
6	Cu(OAc) ₂	DMF, 120 °C	12	98	0.32	[81]
7	CAN supported HY-zeolite	DMF, 110 °C	4	93	0.77	[82]
8	FeCl ₃ -SiO ₂	DMF, 120 °C	12	79	-	[83]
9	Fe ₃ O ₄ @SiO ₂ /aza-crown ether-Cu (II)	PEG-200, 100 °C	2.5	95	38	[62]
10	Md-Pt NPs@AC	DMF, 90 °C, microwave irradiation (140 W)	15	98	23.76	[84]
11	P ₂ O ₅ -SiO ₂	Solvent-Free, 130 °C or ultrasonic sonication, 45 °C	150	93	1.86	[85]
10	Cu-Cytosine@MCM-41	PEG, 120 °C	0.5	96	61.9	This work
11	Ni-Cytosine@MCM-41	PEG, 120 °C	1	92	920	This work

NaN₃ was repeated under optimized condition (Tables 3 and 4, entries 1) and, then, the catalysts were isolated from the reaction solution after completion of each reaction. Based on obtained results from AAS analysis, the amounts of nickel in the fresh and the recovered Ni-Cytosine@MCM-41 were found to be 0.034×10^{-3} mol g⁻¹ and 0.02×10^{-3} mol g⁻¹, respectively. The exact amount of metal content in the recovered catalysts which indicated a good agreement to the fresh catalyst confirmed the heterogeneous nature of these catalysts. Besides, the isolated reaction solutions were analyzed by AAS technique. In this step, the nickel and copper concentrations in the solution were found to be 0.000008 and 0.000006 mmol ml⁻¹, respectively. These analyses confirmed the very low metal leaching of this catalyst and also the heterogeneous nature of Cu-Cytosine@MCM-41 and Ni-Cytosine@MCM-41.

3.6 | Comparison of the catalysts

In order to show the activity of the Cu-Cytosine@MCM-41 and Ni-Cytosine@MCM-41 in comparison to the previously reported catalysts, the results from the [2 + 3] cycloaddition reaction of benzonitrile with sodium azide in the presence of Cu-Cytosine@MCM-41 and Ni-Cytosine@MCM-41 have

been compared to the previously reported ones. The results of this comparison are summarized in Table 9. The products were obtained in higher yields and TOF values in the presence of Cu-Cytosine@MCM-41 and Ni-Cytosine@MCM-41. Therefore, these catalysts are more effective than other catalysts. In addition, homogeneous catalysts which were used in most of the reported methods could not be recovered and reused (Table 9, entries 1, 4–6). Moreover, several of the reported procedures utilized the organic solvents, such as DMF, or employed high temperature (Table 9, entries 4, 11) which are expensive and not environmental-friendly. Meanwhile, PEG was used as a green solvent in the present work. In some procedures, microwave irradiation (Table 9, entry 10) or ultrasonic sonication (Table 9, entry 11) were used in order to prepare the tetrazole derivatives.

4 | CONCLUSIONS

In this study, practical and recoverable heterogeneous catalysts (Cu-Cytosine@MCM-41 and Ni-Cytosine@MCM-41) were synthesized. In addition, their application was reported for the synthesis of 5-substituted 1H-tetrazoles and for the multicomponent reactions to synthesize pyranopyrazoles. All products were obtained in good yields as the turnover frequency (TOF) confirmed the high

efficiency of these catalysts. Cu-Cytosine@MCM-41 and Ni-Cytosine@MCM-41 were characterized by BET, TGA, XRD, TEM, SEM, EDS, WDX, FT-IR and AAS techniques. These catalysts showed good reusability in the described organic reactions.

ACKNOWLEDGMENTS

This work was supported by the research facilities of Ilam University, Ilam, Iran.

ORCID

Mohsen Nikoorazm  <https://orcid.org/0000-0002-4013-0868>

Bahman Tahmasbi  <https://orcid.org/0000-0002-3605-2852>

REFERENCES

- [1] R. R. Langeslay, D. M. Kaphan, C. L. Marshall, P. C. Stair, A. P. Sattelberger, M. Delferro, *Chem. Rev.* **2019**, *119*, 2128. <https://doi.org/10.1021/acs.chemrev.8b00245>
- [2] A. Ghorbani-Choghamarani, P. Moradi, B. Tahmasbi, *J. Iran. Chem. Soc.* **2019**, *16*, 511. <https://doi.org/10.1007/s13738-018-1526-5>
- [3] P. Ju, S. Wu, Q. Su, X. Li, Z. Liu, G. Li, Q. Wu, *J. Mater. Chem. A* **2019**, *7*, 2660. <https://doi.org/10.1039/C8TA11330K>
- [4] Y. Rangraz, F. Nemati, A. Elhampour, *New J. Chem.* **2018**, *42*, 15361. <https://doi.org/10.1039/C8NJ02433B>
- [5] M. Zarei, H. Seprehmansourie, M. A. Zolfigol, R. Karamian, S. H. M. Farida, *New J. Chem.* **2018**, *42*, 14308. <https://doi.org/10.1039/C8NJ02470G>
- [6] S. Moradi, M. A. Zolfigol, M. Zarei, D. A. Alonso, A. Khoshnood, A. Tajally, *Appl. Organomet. Chem.* **2018**, *32*, e4043. <https://doi.org/10.1002/aoc.4043>
- [7] A. Ghorbani-Choghamarani, M. Mohammadi, T. Tamoradi, M. Ghadermazi, *Polyhedron* **2019**, *158*, 25. <https://doi.org/10.1016/j.poly.2018.10.054>
- [8] D. Wang, D. Astruc, *Chem. Rev.* **2014**, *114*, 6949. <https://doi.org/10.1021/cr500134h>
- [9] V. Polshettiwar, R. Luque, A. Fihri, H. Zhu, M. Bouhrara, J. M. Basset, *Chem. Rev.* **2011**, *111*, 3036. <https://doi.org/10.1021/cr100230z>
- [10] Q. Wang, D. Astruc, *Chem. Rev.* **2019**. <https://doi.org/10.1021/acs.chemrev.9b00223>
- [11] A. Ghorbani-Choghamarani, M. Nikoorazm, H. Goudarziafshar, B. Tahmasbi, *Bull. Korean Chem. Soc.* **2009**, *40*, 1388. <https://doi.org/10.1002/chin.200945034>
- [12] Z. B. Shifrina, V. G. Matveeva, L. M. Bronstein, *Chem. Rev.* **2019**. <https://doi.org/10.1021/acs.chemrev.9b00137>
- [13] R. M. Ansari, B. R. Bhat, *Chem. Phys.* **2019**, *517*, 155. <https://doi.org/10.1016/j.chemphys.2018.09.018>
- [14] V. B. Saptal, M. V. Saptal, R. S. Mane, T. Sasaki, B. M. Bhanage, *ACS Omega* **2019**, *4*, 643. <https://doi.org/10.1021/acsomega.8b03023>
- [15] Z. Ghadamyari, A. Shiri, A. Khojastehnezhad, S. M. Seyedi, *Appl. Organomet. Chem.* **2019**, *33*, e5091. <https://doi.org/10.1002/aoc.5091>
- [16] M. Rohaniyan, A. Davoodnia, S. A. Beyramabadi, A. Khojastehnezhad, F. Tajfirooz, *Appl. Organomet. Chem.* **2019**, *33*, e4881. <https://doi.org/10.1002/aoc.4881>
- [17] H. Veisi, A. Nikseresht, N. Ahmadi, K. Khosravi, F. Saeidifar, *Polyhedron* **2019**, *162*, 240. <https://doi.org/10.1016/j.poly.2019.01.070>
- [18] A. Ghorbani-Choghamarani, B. Tahmasbi, N. Noori, S. Faryadi, *C. R. Chim.* **2017**, *20*, 132. <https://doi.org/10.1016/j.crci.2016.06.010>
- [19] S. Y. Chong, T. T. Wang, L. C. Cheng, H. Y. Lv, M. Ji, *Langmuir* **2019**, *35*, 495. <https://doi.org/10.1021/acs.langmuir.8b03153>
- [20] T. T. Nguyen, X. T. T. Nguyen, T. L. H. Nguyen, P. H. Tran, *ACS Omega* **2019**, *4*, 368. <https://doi.org/10.1021/acsomega.8b02932>
- [21] K. Bahrami, M. Khodamorady, *Catal. Lett.* **2019**, *149*, 688. <https://doi.org/10.1007/s10562-018-2627-6>
- [22] A. Ghorbani-Choghamarani, M. Hajjami, B. Tahmasbi, N. Noori, *J. Iran. Chem. Soc.* **2016**, *13*, 2193. <https://doi.org/10.1007/s13738-016-0937-4>
- [23] P. Moradi, M. Hajjami, F. Valizadeh-Kakhki, *Appl. Organomet. Chem.* **2019**, *33*, e5205. <https://doi.org/10.1002/aoc.5205>
- [24] A. Davoodnia, M. Pordel, M. Ebrahimi, A. Khojastehnezhad, *Appl. Organomet. Chem.* **2017**, *31*, e3930. <https://doi.org/10.1002/aoc.3930>
- [25] B. Maleki, S. Barat Nam Chalaki, S. Sedigh Ashrafi, S. Rezaee Seresht, F. Moeinpour, A. Khojastehnezhad, R. Tayebbe, *Appl. Organomet. Chem.* **2015**, *29*, 290. <https://doi.org/10.1002/aoc.3288>
- [26] M. Keyhaniyan, A. Shiri, H. Eshghi, A. Khojastehnezhad, *Appl. Organomet. Chem.* **2018**, *32*, e4344. <https://doi.org/10.1002/aoc.4344>
- [27] M. Nikoorazm, A. Ghorbani-Choghamarani, A. Panahi, B. Tahmasbi, N. Noori, *J. Iran. Chem. Soc.* **2018**, *15*, 181. <https://doi.org/10.1007/s13738-017-1222-x>
- [28] M. Nikoorazm, A. Ghorbani-Choghamarani, M. Khanmoradi, *RSC Adv.* **2016**, *6*, 56549. <https://doi.org/10.1039/C6RA09371J>
- [29] M. Nikoorazm, N. Noori, B. Tahmasbi, S. Faryadi, *Transition Met. Chem.* **2017**, *42*, 469. <https://doi.org/10.1007/s11243-017-0151-y>
- [30] G. Maria, A. I. Stoica, I. Luta, D. Stirbet, G. L. Radu, *Microporous Mesoporous Mater.* **2012**, *162*, 80. <https://doi.org/10.1016/j.micromeso.2012.06.013>
- [31] S. A. Idris, S. R. Harvey, L. T. Gibson, *J. Hazard. Mater.* **2011**, *193*, 171. <https://doi.org/10.1016/j.jhazmat.2011.07.037>
- [32] Y. Sun, X. W. Liu, W. Su, Y. Zhou, L. Zhou, *Appl. Surf. Sci.* **2007**, *253*, 5650. <https://doi.org/10.1016/j.apsusc.2006.12.099>
- [33] A. Benhamou, J. P. Basly, M. Baudu, Z. Derriche, R. Hamacha, *J. Colloid Interface Sci.* **2013**, *404*, 135. <https://doi.org/10.1016/j.jcis.2013.04.026>
- [34] A. Maleki, M. Aghaei, T. Kari, *Polycyclic Aromat. Comp.* **2019**, *39*, 266. <https://doi.org/10.1080/10406638.2017.1325746>
- [35] A. Maleki, J. Rahimi, O. M. Demchuk, A. Z. Wilczewska, R. Jasiński, *Ultrason. Sonochem.* **2018**, *43*, 262. <https://doi.org/10.1016/j.ultsonch.2017.12.047>

- [36] A. Maleki, *Polycyclic Aromat. Comp.* **2018**, *38*, 402. <https://doi.org/10.1080/10406638.2016.1221836>
- [37] A. Maleki, P. Ravaghi, M. Aghaei, H. Movahed, *Res. Chem. Intermed.* **2017**, *43*, 5485. <https://doi.org/10.1007/s11164-017-2941-4>
- [38] A. Maleki, A. Ali Jafari, S. Yousefi, *Carbohydr. Polym.* **2017**, *175*, 409. <https://doi.org/10.1016/j.carbpol.2017.08.019>
- [39] A. Maleki, M. Aghaei, H. R. Hafizi-Atabak, M. Ferdowsi, *Ultrason. Sonochem.* **2017**, *37*, 260. <https://doi.org/10.1016/j.ultrasonch.2017.01.022>
- [40] A. Maleki, Z. Hajizadeh, P. Salehi, *Sci. Rep.* **2019**, *9*, 5552. <https://doi.org/10.1038/s41598-019-42126-9>
- [41] A. Ghorbani-Choghamarani, M. A. Zolfigol, M. Hajjami, H. Goudarziashar, M. Nikoorazm, S. Yousefi, B. Tahmasbi, *J. Braz. Chem. Soc.* **2011**, *22*, 525. <https://doi.org/10.1590/S0103-50532011000300016>
- [42] A. R. Moosavi-Zare, M. A. Zolfigol, F. Derakhshan-Panah, S. Balalaie, *Mol. Catal.* **2018**, *449*, 142. <https://doi.org/10.1016/j.mcat.2017.09.037>
- [43] A. Dömling, W. Wang, K. Wang, *Chem. Rev.* **2012**, *112*, 3083. <https://doi.org/10.1021/cr100233r>
- [44] C. G. Neochoritis, T. Zhao, A. Dömling, *Chem. Rev.* **2019**, *119*, 1970. <https://doi.org/10.1021/acs.chemrev.8b00564>
- [45] A. Maleki, Z. Varzi, F. Hassanzadeh-Afruzi, *Polyhedron* **2019**, *171*, 193. <https://doi.org/10.1016/j.poly.2019.07.016>
- [46] A. Maleki, Z. Hajizadeh, R. Firouzi-Haji, *Microporous Mesoporous Mat.* **2018**, *259*, 46–53. <https://doi.org/10.1016/j.micromeso.2017.09.034>
- [47] L. Zeng, H. Sajiki, S. Cui, *Org. Lett.* **2019**, *21*, 5269. <https://doi.org/10.1021/acs.orglett.9b01871>
- [48] M. R. McKeown, D. L. Shaw, H. Fu, S. Liu, X. Xu, J. J. Marineau, Y. Huang, X. Zhang, D. L. Buckley, A. Kadam, Z. Zhang, S. C. Blacklow, J. Qi, W. Zhang, J. E. Bradner, *J. Med. Chem.* **2014**, *57*, 9019. <https://doi.org/10.1021/jm501120z>
- [49] A. Maleki, M. Aghaei, N. Ghamari, *Appl. Organomet. Chem.* **2016**, *30*, 939. <https://doi.org/10.1002/aoc.3524>
- [50] A. Maleki, E. Akhlaghi, R. Paydar, *Appl. Organomet. Chem.* **2016**, *30*, 382. <https://doi.org/10.1002/aoc.3443>
- [51] M. Wu, Q. Feng, D. Wan, J. Ma, *Synth. Commun.* **2013**, *43*, 1721. <https://doi.org/10.1080/00397911.2012.666315>
- [52] Z. Lu, J. Xiao, D. Wang, Y. Li, *Asian J. Org. Chem.* **2015**, *4*, 487. <https://doi.org/10.1002/ajoc.201500039>
- [53] P. S. Sinija, K. Sree Kumar, *RSC Adv.* **2015**, *5*, 101776. <https://doi.org/10.1039/C5RA16723J>
- [54] B. J. Khairnar, D. V. Mane, B. R. Chaudhari, *J. Applicable Chem.* **2019**, *8*, 425.
- [55] M. Mokhtary, *Iran. J. Catal.* **2019**, *9*, 21.
- [56] M. Koohshari, M. Dabiri, P. Salehi, *RSC Adv.* **2014**, *4*, 10669. <https://doi.org/10.1039/C3RA47639A>
- [57] A. Khazaei, M. A. Zolfigol, F. Karimitabar, I. Nikokar, A. R. Moosavi-Zare, *RSC Adv.* **2015**, *5*, 71402. <https://doi.org/10.1039/C5RA10730J>
- [58] S. A. Hamrahian, S. Salehzadeh, J. Rakhtshah, F. Haji Babaei, N. Karami, *Appl. Organomet. Chem.* **2019**, *33*, e4723. <https://doi.org/10.1002/aoc.4723>
- [59] P. Moradi, A. Ghorbani-Choghamarani, *Appl. Organomet. Chem.* **2017**, *31*, e3602. <https://doi.org/10.1002/aoc.3602>
- [60] P. K. Samanta, R. Biswas, T. Das, M. Nandi, B. Adhikary, R. M. Richards, P. Biswas, *J. Porous Mater.* **2019**, *26*, 145. <https://doi.org/10.1007/s10934-018-0626-z>
- [61] B. Tahmasbi, A. Ghorbani-Choghamarani, *Appl. Organomet. Chem.* **2017**, *31*, e3644. <https://doi.org/10.1002/aoc.3644>
- [62] F. Rezaei, M. Ali Amrollahi, R. Khalifeh, *Inorg. Chim. Acta* **2019**, *489*, 8. <https://doi.org/10.1016/j.ica.2019.01.039>
- [63] P. Akbarzadeh, N. Koukabi, E. Kolvari, *Res. Chem. Intermed.* **2019**, *45*, 1009. <https://doi.org/10.1007/s11164-018-3657-9>
- [64] A. Jabbari, B. Tahmasbi, M. Nikoorazm, A. Ghorbani-Choghamarani, *Appl. Organomet. Chem.* **2018**, *32*, e4295. <https://doi.org/10.1002/aoc.4295>
- [65] A. Maleki, M. Niksefat, J. Rahimi, S. Azadegan, *Polyhedron* **2019**, *167*, 103. <https://doi.org/10.1016/j.poly.2019.04.015>
- [66] A. Sarvary, A. Maleki, *Mol. Diversity* **2015**, *19*, 189. <https://doi.org/10.1007/s11030-014-9553-3>
- [67] A. Maleki, A. Sarvary, *RSC Adv.* **2015**, *5*, 60938. <https://doi.org/10.1039/c5ra11531k>
- [68] X. Xiong, C. Yi, X. Liao, S. Lai, *Tetrahedron Lett.* **2019**, *60*, 402. <https://doi.org/10.1016/j.tetlet.2018.12.037>
- [69] M. Nikoorazm, A. Ghorbani-Choghamarani, M. Khanmoradi, P. Moradi, *J. Porous Mater.* **2018**, *25*, 1831. <https://doi.org/10.1007/s10934-018-0597-0>
- [70] Z. Hajizadeh, A. Maleki, *Mol. Catal.* **2018**, *460*, 87. <https://doi.org/10.1016/j.mcat.2018.09.018>
- [71] A. R. Moosavi-Zare, M. A. Zolfigol, A. Mousavi-Tashar, *Res. Chem. Intermed.* **2016**, *42*, 7305. <https://doi.org/10.1007/s11164-016-2537-4>
- [72] M. Nikoorazm, A. Ghorbani-Choghamarani, N. Noori, B. Tahmasbi, *Appl. Organomet. Chem.* **2016**, *30*, 843. <https://doi.org/10.1002/aoc.3512>
- [73] A. Ghorbani-Choghamarani, P. Moradi, B. Tahmasbi, *Polyhedron* **2019**, *163*, 98. <https://doi.org/10.1016/j.poly.2019.02.004>
- [74] T. Tamoradi, M. Ghadermazi, A. Ghorbani-Choghamarani, *Catal. Lett.* **2018**, *148*, 857. <https://doi.org/10.1007/s10562-018-2311-x>
- [75] T. Tamoradi, M. Ghadermazi, A. Ghorbani-Choghamarani, *New J. Chem.* **2018**, *42*, 5479. <https://doi.org/10.1039/C7NJ05189A>
- [76] M. Nikoorazm, Z. Rezaei, B. Tahmasbi, *J. Porous Mater.* **2020**, *27*, 671–689. <https://doi.org/10.1007/s10934-019-00835-6>
- [77] S. Kumar, S. Dubey, N. Saxena, S. K. Awasthi, *Tetrahedron Lett.* **2014**, *55*, 6034. <https://doi.org/10.1016/j.tetlet.2014.09.010>
- [78] F. Dehghani, A. R. Sardarian, M. Esmaeilpour, *J. Organomet. Chem.* **2013**, *743*, 87. <https://doi.org/10.1016/j.jorganchem.2013.06.019>
- [79] W. X. Wang, H. L. Cai, R. G. Xiong, *Chin. Chem. Lett.* **2013**, *24*, 783. <https://doi.org/10.1016/j.ccllet.2013.04.041>
- [80] P. Mani, A. K. Singh, S. K. Awasthi, *Tetrahedron Lett.* **2014**, *55*, 1879. <https://doi.org/10.1016/j.tetlet.2014.01.117>
- [81] U. B. Patil, K. R. Kumthekar, J. M. Nagarkar, *Tetrahedron Lett.* **2012**, *53*, 3706. <https://doi.org/10.1016/j.tetlet.2012.04.093>
- [82] P. Sivaguru, K. Bhuvaneshwari, R. Ramkumar, A. Lalitha, *Tetrahedron Lett.* **2014**, *55*, 5683. <https://doi.org/10.1016/j.tetlet.2014.08.066>

- [83] M. Nasrollahzadeh, Y. Bayat, D. Habibi, S. Moshaei, *Tetrahedron Lett.* **2009**, *50*, 4435. <https://doi.org/10.1016/j.tetlet.2009.05.048>
- [84] E. Erken, İ. Esirden, M. Kaya, F. Sen, *RSC Adv.* **2015**, *5*, 68558. <https://doi.org/10.1039/C5RA11426H>
- [85] D. Habibi, M. Nasrollahzadeh, L. Mehrabi, S. Mostafaei, *Monatsh. Chem.* **2013**, *144*, 725. <https://doi.org/10.1007/s00706-012-0871-9>

How to cite this article: Nikoorazm M, Tahmasbi B, Gholami S, Moradi P. Copper and nickel immobilized on cytosine@MCM-41: as highly efficient, reusable and organic-inorganic hybrid nanocatalysts for the homoselective synthesis of tetrazoles and pyranopyrazoles. *Appl Organomet Chem.* 2020;e5919. <https://doi.org/10.1002/aoc.5919>

SUPPORTING INFORMATION

Additional supporting information may be found online in the Supporting Information section at the end of this article.